Journal of the European Ceramic Society xxx (xxxx) xxx

Contents lists available at ScienceDirect

Journal of the European Ceramic Society

journal homepage: www.elsevier.com/locate/jeurceramsoc

Synthesis and properties of blue zirconia ceramic based on Ni/Co doped $Ba_{0.956}Mg_{0.912}Al_{10.088}O_{17}$ blue pigments

Qiuyu Cheng [a], Xin Chen [a], Peng Jiang [a,*], Qiuying Wang [a], Zhiwei Wang [a], M.A. Subramanian [b]

[a] Department of Inorganic Nonmetallic Materials, School of Materials Science and Engineering, University of Science and Technology Beijing, Beijing 100083, China
[b] Department of Chemistry, Oregon State University, Corvallis, OR 97330, USA

ARTICLE INFO

Keywords:
β-alumina structure
Blue pigment
Optical properties
Blue zirconia ceramic

ABSTRACT

Novel blue pigments based on $Ba_{0.956}Mg_{0.912}Al_{10.088-x}Ni_xO_{17}$ ($0 \leq x \leq 0.3$) and $Ba_{0.956}Mg_{0.912}Al_{10.088-x}Co_xO_{17}$ ($0 \leq x \leq 0.3$) solid solutions were successfully synthesized by solid state method. The XRD results confirmed the structure of the as-synthesized sample belongs to hexagonal β-alumina structure with the space group of $P6_3/mmc$. The *d-d* electron transitions in Ni^{2+}/Co^{2+} tetrahedral sites in the visible light range are the reason for the blue colors. Then, the as-prepared blue oxides were sintered with ZrO_2 powders at 1400 °C to prepare blue zirconia ceramic materials. Based on XRD and SEM analysis, the pigment phase is stable after high-temperature sintering with ZrO_2, and a clear grain boundary is observed. The XCT results indicate the prepared blue ceramics are dense and very small pores are rarely distributed inside the blue zirconia ceramic body. Additionally, the mechanical properties of the fabricated blue ceramics were maintained compared to pure ZrO_2 ceramic.

1. Introduction

Zirconia (ZrO_2) ceramics are indispensable structural and functional materials due to their outstanding physical and chemical properties such as high strength, excellent hardness, chemical safety, stability, and so forth [1]. In addition to white ceramics, colored ceramics have also been developed and are widely used for decorations such as watches, bracelets, and cell phone back panels for their unique properties of beautiful colors, metallic lusters. Moreover, they are almost allergy-free to users sensitive to metals [2]. However, as a result of the high sintering temperature (~1500 °C) of ZrO_2, only a few pigments are compatible in zirconia. Therefore, expanding the color range of colored zirconia ceramics with saturated color and stable phase is very attractive and in great demand.

Transition metal elements are widely used in the development of colored zirconia ceramics. For example, Ren et al. reported that V-doped ZrO_2 appears a yellow color, where the color is originated in V^{4+} substitution into ZrO_2 lattice [3]. Other colored ZrO_2 with various colors, such as Cr/Co-ZrO_2 green ceramics [4] and Ti-ZrO_2 black zirconia ceramics are successfully prepared under the same mechanism [5]. However, the precise control of the transition metal substitution is very difficult. Therefore, the uniformity and repeatability of its apparent color are not satisfied, which are not qualified for daily application. Rare earth oxides dispersed in ZrO_2 can obtain colored zirconia ceramics. For instance, Nb_2O_3 was used as a colorant to prepare purple zirconia ceramics by solid state method [2], and CeO_2 doped red zirconia ceramics were prepared by a high-temperature reduction method [6]. In these cases, the rare-earth oxides are expensive, which makes them hard to be widely applied.

Recent researches show that certain complex oxide as a pigment phase will be stable after high-temperature sintering with ZrO_2. Zhang et al. reported that both $ErAlO_3$ with a perovskite structure and $Er_3Al_5O_{12}$ with a garnet structure successfully tuned the zirconia to pink color through a gel-polymerization method at 1100 °C. When the sintered temperature is above 1200 °C, neither $ErAlO_3$ nor $Er_3Al_5O_{12}$ cloud stably exist in the zirconia matrix as the color oxides decomposed to Er^{3+} which enters to ZrO_2 lattice and colored the ceramic [7]. In this case, the color mechanism is as same as the transition metal substitution, which leads to poor uniformity and repeatability of its apparent color. Oxides with spinel structure are widely used in color generation and some are reported successfully used in zirconia coloration. A black zirconia ceramic was prepared using (Co, Zn)Fe_2O_4 as a colorant by solid state method [8]. For blue zirconia, the widely used pigment is $CoAl_2O_4$ (cobalt blue). Its preparation involves a high temperature solid-state reaction of mechanically mixing cobalt blue as the second phase in zirconia. The amount of Co used in cobalt blue is 33.32 wt%, and 1.66 wt

* Corresponding author.
E-mail address: jiangp@ustb.edu.cn (P. Jiang).

https://doi.org/10.1016/j.jeurceramsoc.2022.04.015
Received 24 November 2021; Received in revised form 15 March 2022; Accepted 8 April 2022
Available online 11 April 2022

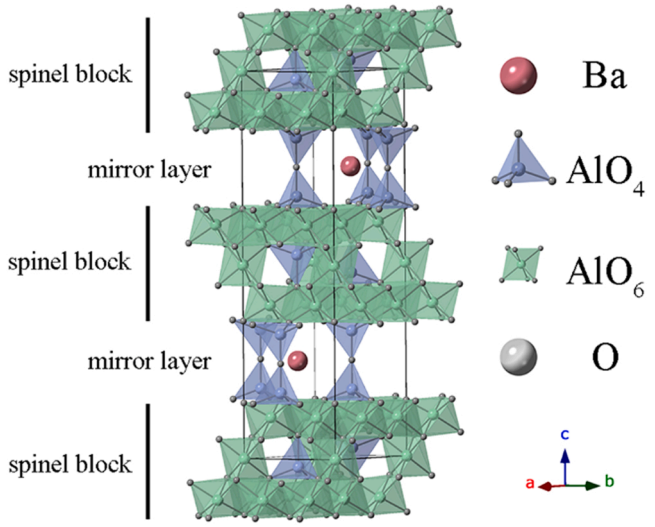

Fig. 1. Crystal structure of $BaMgAl_{10}O_{17}$.

% in the prepared 5 wt% $CoAl_2O_4$ zirconia ceramic. Due to the facts that Co is harmful to the human body and environment, as well as its storage is rare, it is important to find other blue pigments which can eliminate or reduce the amount of Co used in the blue zirconia ceramics. As the blue color of $CoAl_2O_4$ is derived from its spinel structure in which Co^{2+} resides in the tetrahedral sites, similar spinel blocks with Co^{2+} are able to produce intense blue colors with higher opportunity. By this way, the doping concentration of Co is possibly reduced by the introduction of the other ions. At the same time, the vivid color and high-temperature stability brought by the spinel structure could be maintained.

$BaMgAl_{10}O_{17}$ demonstrates a hexagonal β-alumina structure with the space group of $P6_3/mmc$. As shown in Fig. 1, its structure contains two spinel blocks ($MgAl_{10}O_{16}$) separated by a mirror layer (BaO). In this structure, doping of rare earth elements or transition metal ions in the spinel blocks was proved to bring interesting luminescent properties. Eu-doped $BaMgAl_{10}O_{17}$ was reported as one of the most significant blue-emission phosphors, which has been utilized in plasma display panels (PDPs) [9]. Cr-doped $BaMgAl_{10}O_{17}$ are red-emitting phosphors that could be applied in plant growth LED [10], and Mn-doped $BaMgAl_{10}O_{17}$ is representative commercial green phosphor [11]. The coexistence of rare earth element and transition metal ion in $BaMgAl_{10}O_{17}$ was also synthesized and evaluated for luminescent applications. $Ba_{1-m}Eu_mMg_{1-n}Co_nAl_{10}O_{17}$ ($0 \le m \le 0.14$ and $0 \le n \le 0.01$) compound was designed and synthesized by conventional solid state reaction in air. It was found that a limited amount of Co is helpful to enhance the luminescent properties of Eu-$BaMgAl_{10}O_{17}$ [12]. Samples with one Co dopant were also synthesized with a very limited amount ($0 \le n \le 0.01$ in the chemical formula) and their UV-Vis absorbance spectra are provided and analyzed. However, as Co-doped samples did not show excellent luminescent properties with enhanced Co doping concentration, a higher amount of Co in $BaMgAl_{10}O_{17}$ was not tried or comprehensively studied for pigment applications. Though the colors of

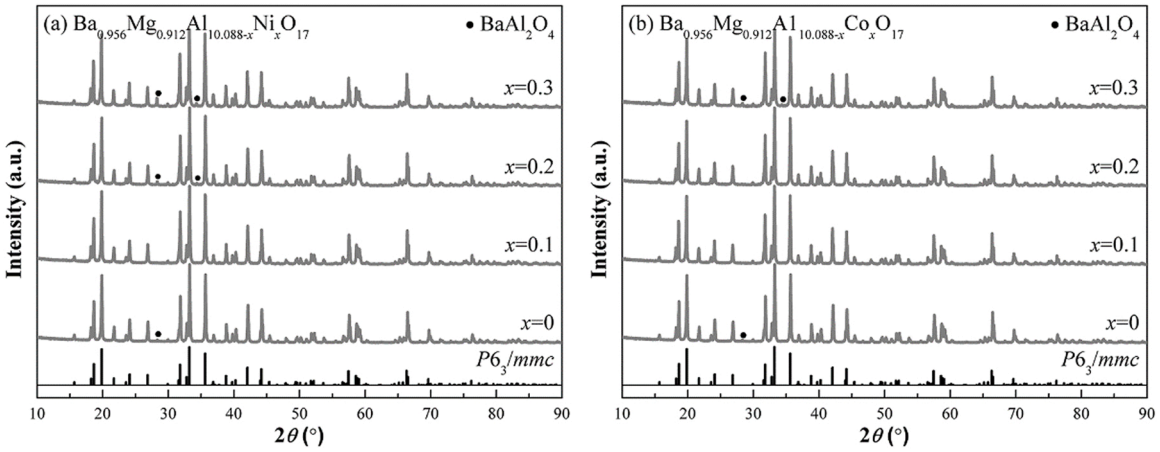

Fig. 2. XRD patterns of (a) $Ba_{0.956}Mg_{0.912}Al_{10.088-x}Ni_xO_{17}$ ($0 \le x \le 0.3$) and (b) $Ba_{0.956}Mg_{0.912}Al_{10.088-x}Co_xO_{17}$ ($0 \le x \le 0.3$) synthesized powders.

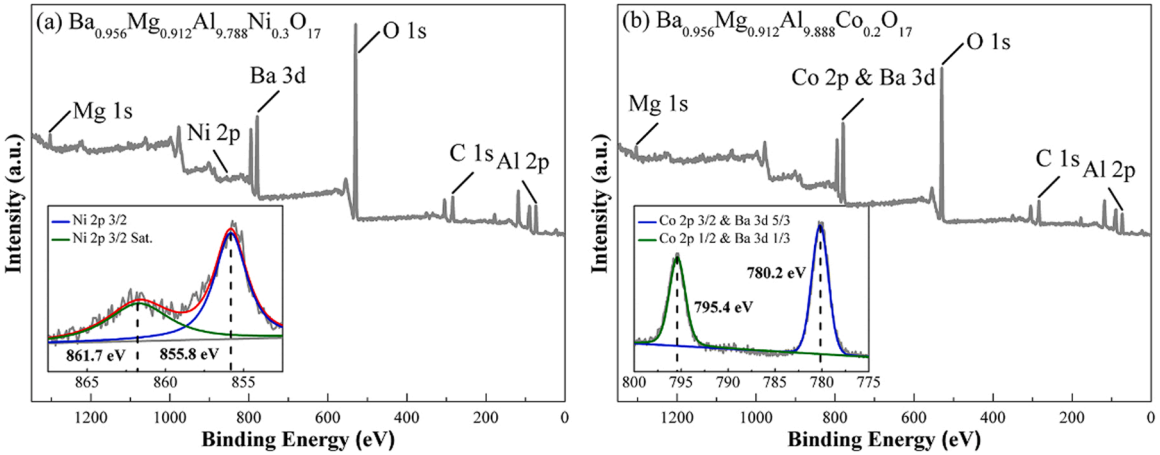

Fig. 3. XPS spectra of (a) $Ba_{0.956}Mg_{0.912}Al_{9.788}Ni_{0.3}O_{17}$ and (b) $Ba_{0.956}Mg_{0.912}Al_{9.888}Co_{0.2}O_{17}$ synthesized powders.

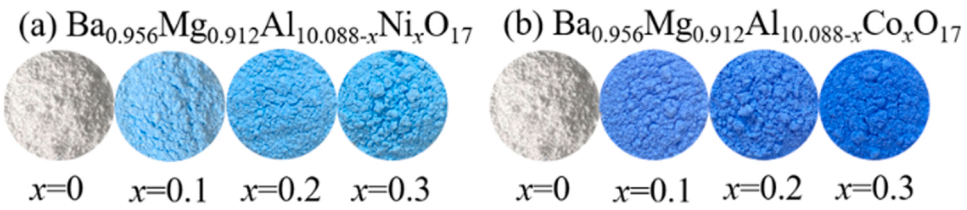

Fig. 4. The apparent colors of (a) $Ba_{0.956}Mg_{0.912}Al_{10.088-x}Ni_xO_{17}$ ($0 \le x \le 0.3$) and (b) $Ba_{0.956}Mg_{0.912}Al_{10.088-x}Co_xO_{17}$ ($0 \le x \le 0.3$) synthesized powders.

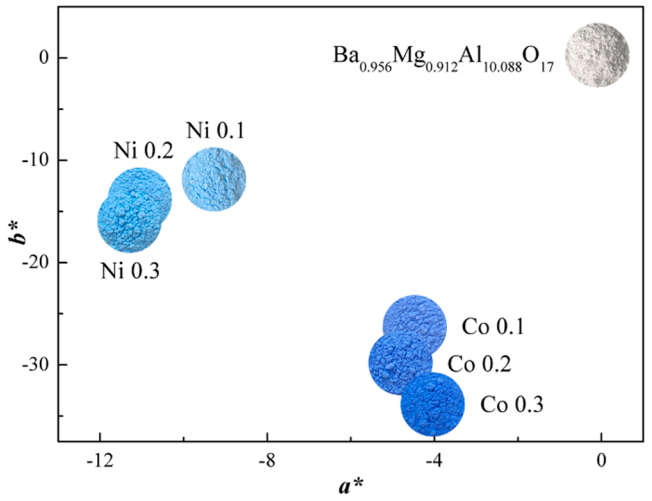

Fig. 5. Color coordinates with digital photos of as-synthesized pigments powders in a^*b^* space.

Co-$BaMgAl_{10}O_{17}$ samples were not provided, the blue color was mentioned in the research which indicates great potential as a blue pigment.

Unfortunately, it was found that the synthesis of samples with higher Co is restricted as impurity phases will appear [12]. Previous reports also showed that even the pure phase of $BaMgAl_{10}O_{17}$ is difficult to achieve. Impurities such as $BaAl_2O_4$ and Al_2O_3 phases with relatively high intensity were always accompanied in their X-ray diffraction patterns [10]. However, the synthesis of pigment with intense color normally requires a higher amount of transition metal concentration. Therefore, in order to obtain a promising pigment from $BaMgAl_{10}O_{17}$, the elimination of impurity phases when doping with transition metal ion is necessary. $BaMgAl_{10}O_{17}$ crystalizes in β-alumina structure which usually exhibits nonstoichiometric compositions such as $Ba_{0.75}Al_{11}O_{17.25}$ and $Ba_{1.167}Al_{10.667}O_{17.167}$ [13]. In 1986, Iyi et al. [14] reported that the composition of Ba β-alumina was proved as $Ba_{0.956}Mg_{0.912}Al_{10.088}O_{17}$ by single crystal growth and analysis. In the non-stoichiometric formula of $Ba_{0.956}Mg_{0.912}Al_{10.088}O_{17}$, Ba is in deficiency while some Mg^{2+} is substituted by Al^{3+} in the spinel block to maintain the charge balance. As the structure favors a lower amount of bigger Ba^{2+} ions, $Ba_{0.956}Mg_{0.912}Al_{10.088}O_{17}$, which may help to better eliminate the impurities, was selected as the target compound to dope transition metal ions for pigment synthesis.

In this study, Ni/Co doped $Ba_{0.956}Mg_{0.912}Al_{10.088}O_{17}$ blue pigments were prepared by a conventional solid state reaction. Then, a series of blue zirconia ceramics containing 5 wt% and 10 wt% as-synthesized blue pigments were prepared via a solid state method. In addition, the structure and properties of the synthesized blue pigments and the colored zirconia ceramics were analyzed by XRD, XPS, FESEM, and UV-Vis-NIR spectrophotometer.

2. Experimental

2.1. Preparation of blue pigments

The conventional solid state reaction was used to synthesize the $Ba_{0.956}Mg_{0.912}Al_{10.088-x}Ni_xO_{17}$ ($0 \le x \le 0.3$) and $Ba_{0.956}Mg_{0.912}Al_{10.088-x}Co_xO_{17}$ ($0 \le x \le 0.3$) blue pigments using a stoichiometric weight ratio of $BaCO_3$ (99.95% purity, Aladdin, China), MgO (99.99% purity, Aladdin, China), Al_2O_3 (99.99% purity, Aladdin, China), NiO (99.0% purity, Aladdin, China), and Co_3O_4 (99.95% purity, Aladdin, China). The raw materials were ground using agate mortar with a pestle for 20 min. Next, the mixed powder was pressed into pellets under an applied pressure of 10 MPa for 1 min. After that, the pellets were loaded into alumina crucibles and sintered at 1600 °C for 4 h in an N_2 atmosphere. $CoAl_2O_4$ powders were prepared by solid state method with sintering at 1400 °C for 2 h.

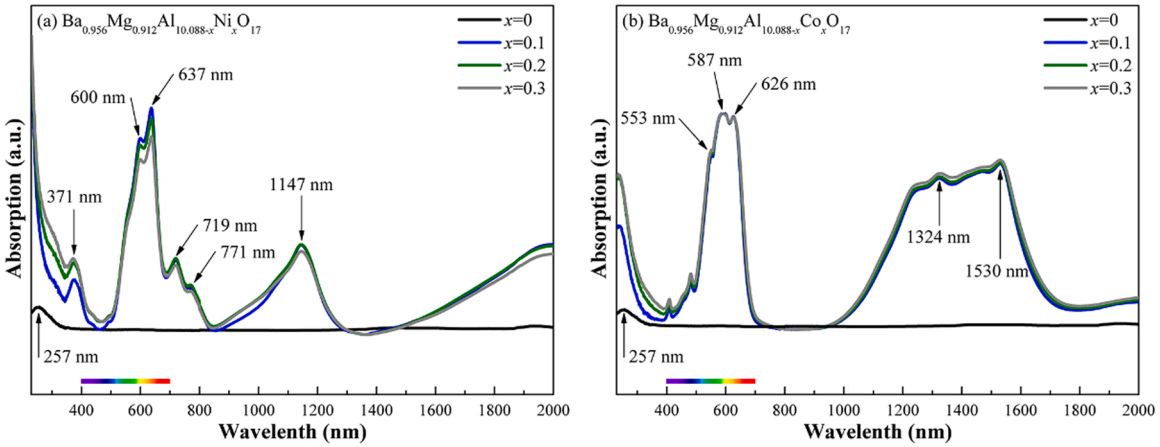

Fig. 6. UV-Vis-NIR absorbance spectra of (a) $Ba_{0.956}Mg_{0.912}Al_{10.088-x}Ni_xO_{17}$ ($0 \le x \le 0.3$) and (b) $Ba_{0.956}Mg_{0.912}Al_{10.088-x}Co_xO_{17}$ ($0 \le x \le 0.3$) synthesized powders.

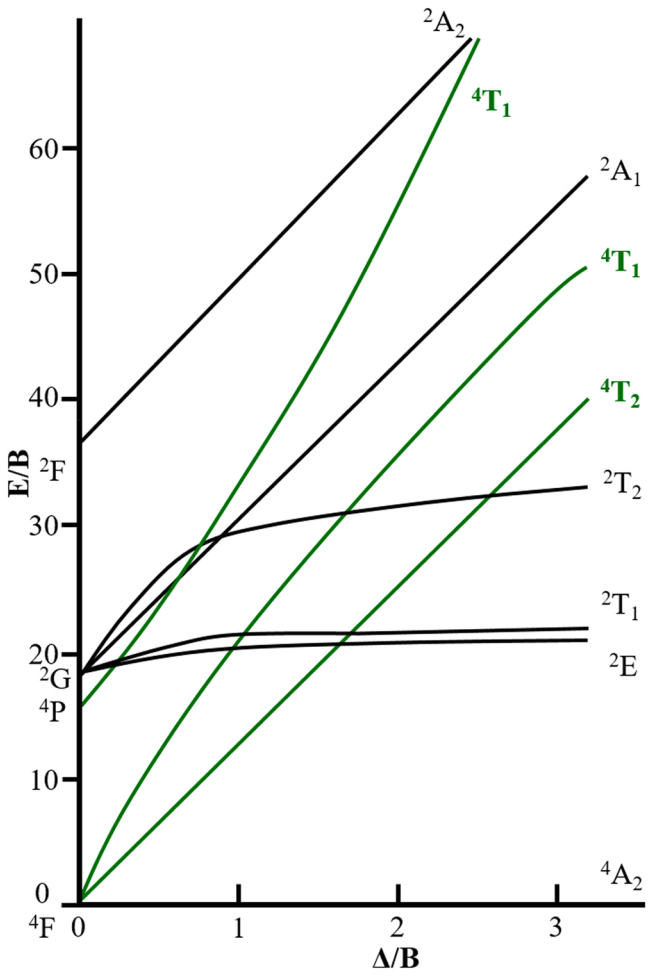

Fig. 7. Tanabe-Sugano (T-S) diagram for Co^{2+} (d^7 electronic configuration) in tetrahedral coordination.

2.2. Preparation of blue zirconia ceramics

The synthesized $Ba_{0.956}Mg_{0.912}Al_{9.988}Ni_{0.1}O_{17}$, $Ba_{0.956}Mg_{0.912}Al_{9.888}Co_{0.2}O_{17}$, and $CoAl_2O_4$ blue pigments powders were added to yttria-stabilized zirconia (YSZ) powder (5 wt% YSZ, 99.99% purity, Jiangxi Size Materials Co., Ltd., China) in the proportions of 5 wt% and 10 wt%, and the blue zirconia ceramics were prepared by the solid state method. They were weighed and dry ball-milled by a bench-top planetary automatic ball mill (MSK-SFM-1) at 300 rpm for 600 min, and then wet ball-milled using ethanol for 30 min. Then, the samples were dried in an oven at 60 °C and held for 12 h. Finally, the mixture was ground, pelleted, and sintered at 1400 °C for 6 h in the air.

2.3. Characterization

X-ray diffraction (XRD) patterns were obtained with a Rigaku Ultima IV X-ray diffractometer using a Cu Kα (λ = 1.5406 Å) radiation in the 2θ range of 10–90° under the working condition of 40 kV and 40 mA.

The oxidation states of Ni/Co in $Ba_{0.956}Mg_{0.912}Al_{10.088}O_{17}$ were obtained by X-ray photoelectron spectroscopy (XPS, ESCALAB 250XI).

The as-fired 5 wt% $Ba_{0.956}Mg_{0.912}Al_{9.988}Ni_{0.1}O_{17}$ and 5 wt% $Ba_{0.956}Mg_{0.912}Al_{9.888}Co_{0.2}O_{17}$ blue zirconia ceramics were polished, and then were thermally etched at 1400 °C for 30 min. After that, the morphology analysis and chemical composition of the as-prepared blue zirconia ceramics were studied by field emission scanning electron microscope (FESEM, JSM-7001 F) combined with an energy dispersive spectrometer (EDS, X-Max).

X-ray Computed Tomography (XCT) analysis by an FF35 industrial CT scanner (YXLON, Germany) was applied to measure the pore distribution of zirconia ceramics with a volume of 1.5 × 1.5 × 5 mm^3, and the scanning time for each sample was approximately 1.5 h.

Vickers microhardness (HV) was measured on the polished zirconia ceramics by Vickers hardness tester (EM-1500 L) at a load of 300 GF and a holding time of 15 s. For each sample, 14 points were tested and recorded, and a proper distance must be maintained between the indentations to avoid interference.

The L^* a^* b^* color parameters of pigments powder and as-fired zirconia ceramic surface were obtained using a benchtop spectrometer (X-Rite Ci7600). For this CIE L^* a^* b^* system, L^* is the color lightness (L^* = 0 for black and 100 for white); $a^* < 0$ indicates green, and $a^* > 0$ indicates red; $b^* < 0$ represents blue, and $b^* > 0$ represents yellow.

The UV-Vis-NIR absorbance spectra of blue pigments and zirconia ceramics were acquired in the wavelength range of 250–2000 nm at room temperature with a UV-Vis-NIR spectrophotometer (Hitachi UH4150), where barium sulfate ($BaSO_4$) was employed as white reference.

3. Results and discussion

3.1. Analysis of blue pigments

3.1.1. XRD analysis

The XRD patterns of the as-synthesized blue pigments are illustrated in Fig. 2. As shown, all the diffraction peaks are sharp and well-indexed to the hexagonal structure of $Ba_{0.956}Mg_{0.912}Al_{10.088}O_{17}$ with the space group of $P6_3/mmc$, indicating Ni/Co doped $Ba_{0.956}Mg_{0.912}Al_{10.088}O_{17}$

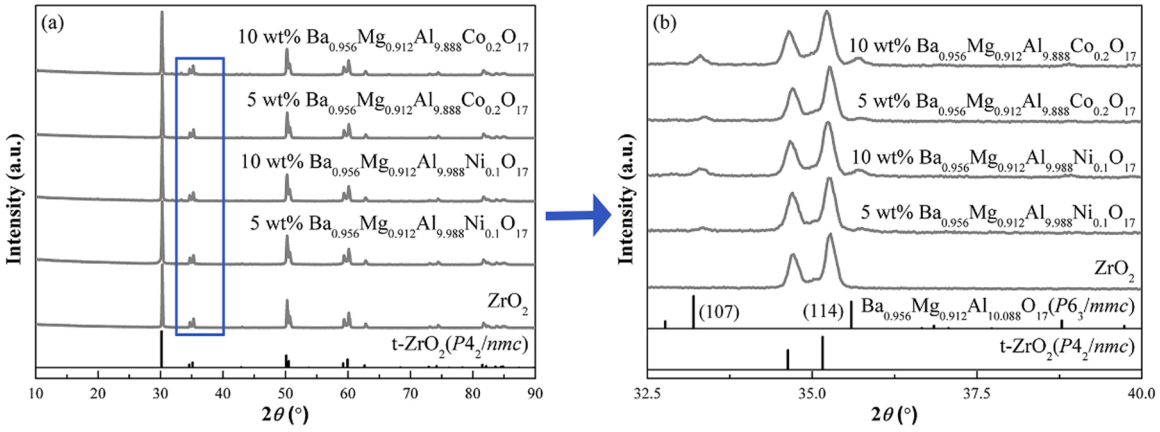

Fig. 8. XRD patterns of as-fired zirconia ceramics.

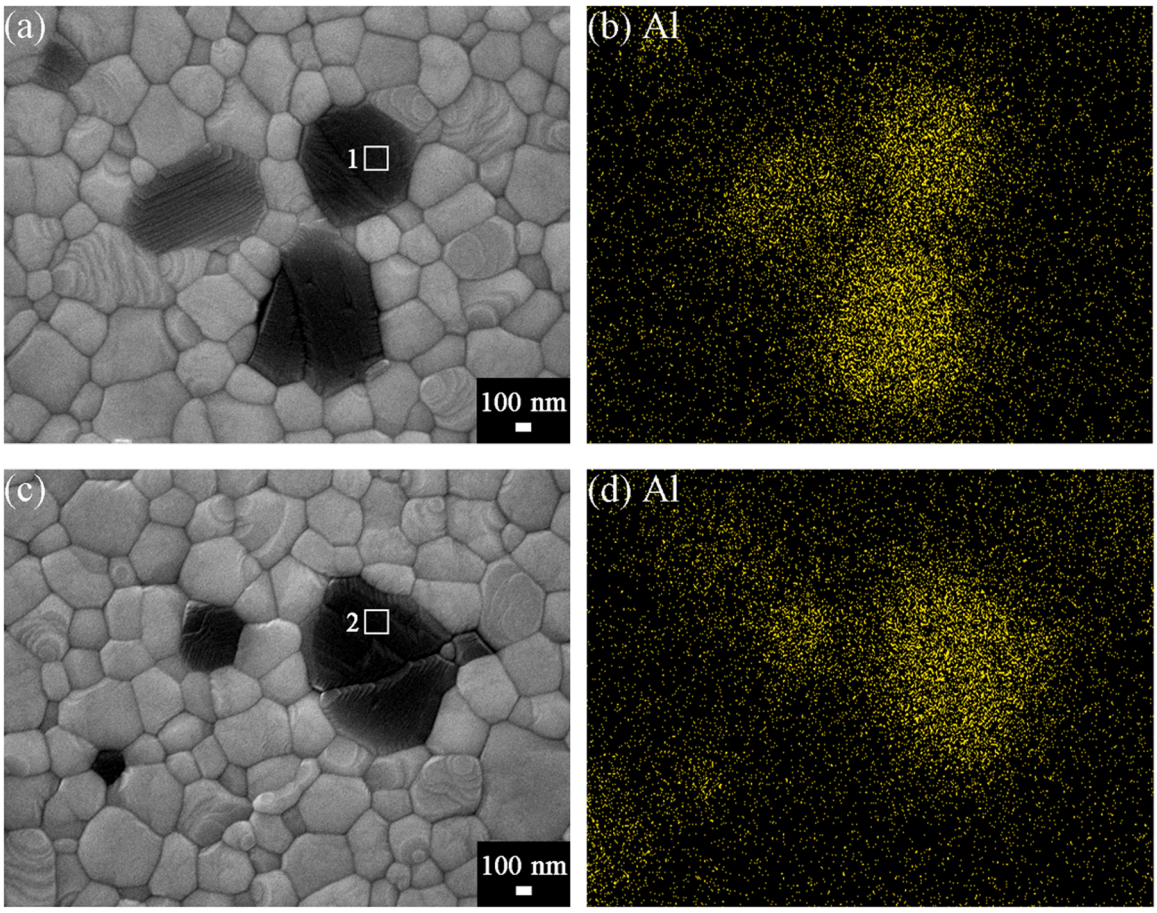

Fig. 9. The polished blue ceramic surface of (a) 5 wt% $Ba_{0.956}Mg_{0.912}Al_{9.988}Ni_{0.1}O_{17}$, (b) EDS elemental mapping 1 of Al; (c) 5 wt% $Ba_{0.956}Mg_{0.912}Al_{9.888}Co_{0.2}O_{17}$, (d) EDS elemental mapping 2 of Al.

Table 1
Multi-elemental atomic percentage (Unit: %) of points 1–2.

Element	Ba	Mg	Al	Ni	Co	Zr	O	Total
1	2.12	1.67	19.98	0.00		15.37	60.68	100
2	2.35	1.68	20.58		0.00	15.29	60.10	100

compounds are successfully synthesized through solid state reaction. When $x = 0$, the observed peak at 28.3° corresponds to (102) planes that could be indexed to the phase of hexagonal $BaAl_2O_4$ (space group: $P6_322$). For Ni-doped samples (Fig. 2a), $Ba_{0.956}Mg_{0.912}Al_{9.988}Ni_{0.1}O_{17}$ is observed as a single phase. Small peaks corresponding to $BaAl_2O_4$ impurity exist when $x = 0.2$, and 0.3. As presented in Fig. 2b, $Ba_{0.956}Mg_{0.912}Al_{9.988}Co_{0.1}O_{17}$ and $Ba_{0.956}Mg_{0.912}Al_{9.888}Co_{0.2}O_{17}$ are observed as single phase. The $BaAl_2O_4$ impurity appears in the samples with higher Co concentrations ($x = 0.3$).

3.1.2. XPS analysis

The XPS spectra of $Ba_{0.956}Mg_{0.912}Al_{9.788}Ni_{0.3}O_{17}$ and $Ba_{0.956}Mg_{0.912}Al_{9.888}Co_{0.2}O_{17}$ are shown in Fig. 3. According to Fig. 3a, in $Ba_{0.956}Mg_{0.912}Al_{9.788}Ni_{0.3}O_{17}$, the binding energy of Ni consists of a main 2p 3/2 peak at 855.6 eV and an associated satellite peak at 861.7 eV. A similar circumstance is observed in $Ni(OH)_2$, in which the main peak is located at 856.2 eV and the satellite peak is located at 861.2 eV [15]. It is reported that the valence of Ni is + 2 in both $Ba_{0.75}Ni_{0.2}Al_{11.8}O_{19-\delta}$ (855.7 eV) [16] and $BaAl_{11.3}Ni_{0.7}O_{19}$ (855.99 eV) [17]. In addition, the structure of $BaAl_{12}O_{19}$ also belongs to the β-alumina. Therefore, the oxidation state of Ni in $Ba_{0.956}Mg_{0.912}Al_{9.788}Ni_{0.3}O_{17}$ is proved to be + 2 valence.

The Co 2p core-level spectrum is characterized by two components due to spin-orbital splitting: Co 2p 3/2 and Co 2p 1/2. Based on previous studies [18], the binding energy of Co 2p 3/2 and Ba 3d 5/2 will possibly overlap. Fig. 3b shows the peaks of Co 2p orbit overlaps with Ba 3d orbit at 780.2 eV and 795.4 eV. The binding energy for Co 2p 3/2 (780.2 eV) is consistent with the value reported for Co^{2+} in CoO (780 eV) [19], CoOOH (780.1 eV) [20], and $Al_{2-x}Co_xTiO_5$ (780.67 eV) [21]. So the oxidation state of Co in $Ba_{0.956}Mg_{0.912}Al_{9.888}Co_{0.2}O_{17}$ presents + 2 valence.

3.1.3. Optical properties

The apparent colors of pigments powder are demonstrated in Fig. 4. The undoped $Ba_{0.956}Mg_{0.912}Al_{10.088}O_{17}$ sample presents a pure white color. When Ni is introduced (Fig. 4a), the color changes to sky blue ($x = 0.1$). A deeper blue hue is observed with an elevated amount of Ni in the compound. In the case of Co substitution, the color of $Ba_{0.956}Mg_{0.912}Al_{10.088-x}Co_xO_{17}$ series (Fig. 4b) varies from light blue ($x = 0.1$) to ocean blue ($x = 0.3$).

The color coordinates with objective colors in a^*b^* space of blue pigments are presented in Fig. 5. In both $Ba_{0.956}Mg_{0.912}Al_{10.088-x}Co_xO_{17}$ ($0 \le x \le 0.3$) and $Ba_{0.956}Mg_{0.912}Al_{10.088-x}Ni_xO_{17}$ ($0 \le x \le 0.3$) pigments, the value of b^* shows a decreasing trend with the doping amount changing from 0.1 to 0.3, indicating the blueness increases. The b^* values in the Co-doped series are lower than that in the Ni-doped series, which suggests a deeper blue color is obtained by Co doping. Besides, the a^* value fluctuated slightly in each blue series, which means that the greenness varies slightly.

The optical spectra of $Ba_{0.956}Mg_{0.912}Al_{10.088-x}Ni_xO_{17}$ ($0 \le x \le 0.3$) and $Ba_{0.956}Mg_{0.912}Al_{10.088-x}Co_xO_{17}$ ($0 \le x \le 0.3$) blue pigments are

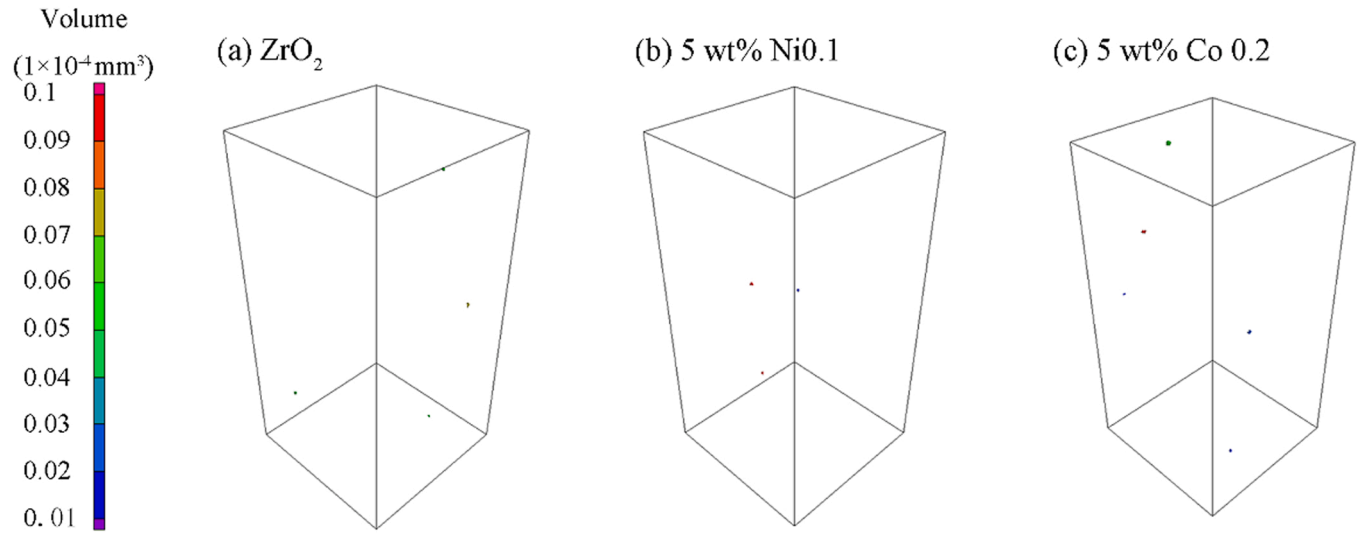

Fig. 10. Pore distribution of as-fired (a) pure ZrO_2 ceramic as well as blue zirconia ceramics of (b) 5 wt% $Ba_{0.956}Mg_{0.912}Al_{9.988}Ni_{0.1}O_{17}$ and (c) 5 wt% $Ba_{0.956}Mg_{0.912}Al_{9.888}Co_{0.2}O_{17}$.

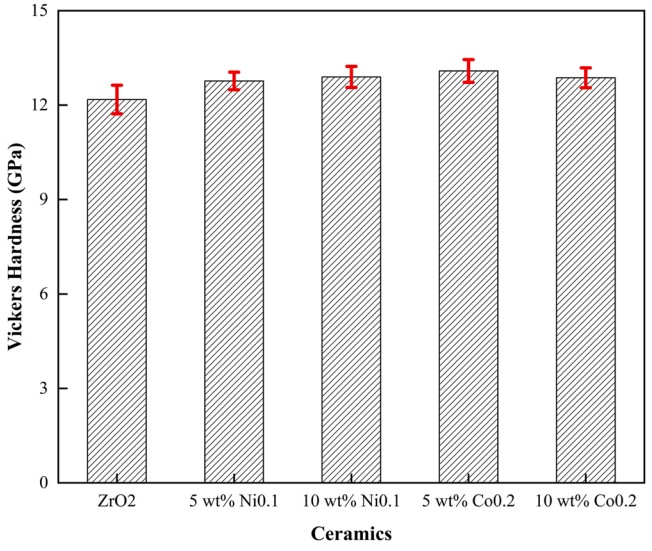

Fig. 11. The average Vickers hardness and the standard deviation to each point of polished zirconia ceramics.

Table 2
The average Vickers hardness and the standard deviation to each point of polished zirconia ceramics.

Ceramic	Average (GPa)	Standard Deviation (GPa)
ZrO_2	12.18	0.46
5 wt% $Ba_{0.956}Mg_{0.912}Al_{9.988}Ni_{0.1}O_{17}$ + 95 wt % ZrO_2	12.77	0.28
10 wt% $Ba_{0.956}Mg_{0.912}Al_{9.988}Ni_{0.1}O_{17}$ + 90 wt% ZrO_2	12.89	0.33
5 wt% $Ba_{0.956}Mg_{0.912}Al_{9.888}Co_{0.2}O_{17}$ + 95 wt% ZrO_2	13.09	0.36
10 wt% $Ba_{0.956}Mg_{0.912}Al_{9.888}Co_{0.2}O_{17}$ + 95 wt% ZrO_2	12.87	0.32

shown in Fig. 6a-b, respectively. The white $Ba_{0.956}Mg_{0.912}Al_{10.088}O_{17}$ powder exhibit an absorption peak at 257 nm that can be assigned to the charge transfer of Al-O bond, while negligible absorption is observed across the entire visible range [22]. The profiles of $Ba_{0.956}Mg_{0.912}Al_{10.088-x}Ni_xO_{17}$ (Fig. 6a) are following the features of Ni^{2+} doped $CaAl_{12}O_{19}$ [23] and $CaNi_xTi_xAl_{12-2x}O_{19}$ [24], in which the absorptions are rooted in Ni^{2+} *d-d* transitions in tetrahedral coordination. Ni^{2+} owns a $3d^8$-configuration, three spin-allowed transitions can be expected for the tetrahedral Ni^{2+}: $^3T_1(F)\rightarrow{}^3T_2(F)$, $^3T_1(F)\rightarrow{}^3A_2(F)$, and $^3T_1(F)\rightarrow{}^3T_1(P)$. Among these transitions, $^3T_1(F)\rightarrow{}^3T_1(P)$ transition is the only spin-allowed transition in the visible region. Therefore, a doublet band of Ni^{2+} with absorption peaks at 600 nm and 637 nm can be attributed to $^3T_1(F)\rightarrow{}^3T_1(P)$ and are responsible for the sky blue color. The near-infrared peak centered at 1147 nm is assigned to $^3T_1(F)\rightarrow{}^3A_2(F)$. Weaker bands of 371 nm, 719 nm, and 771 nm are related to spin-forbidden transitions from $^3T_1(F)$ to $^1A_1(G)$, $^1E_1(D)$, and $^1T_2(D)$, respectively.

Co^{2+} has a $3d^7$-configuration that presents three spin-allowed transitions in both octahedral and tetrahedral ligand fields. In the case of Co^{2+} transitions in a tetrahedral ligand field, the spin allowed transitions are $^4A_2(F)\rightarrow{}^4T_2(F)$, $^4A_2(F)\rightarrow{}^4T_1(F)$, and $^4A_2(F)\rightarrow{}^4T_1(P)$. When considering Co^{2+} in an octahedral ligand field, three spin allowed transitions are $^4T_1(F)\rightarrow{}^4T_2(F)$, $^4T_1(F)\rightarrow{}^4A_2(F)$, and $^4T_1(F)\rightarrow{}^4T_1(P)$. The specific band of octahedral Co^{2+} is the spin-allowed transition $^4T_1(F)\rightarrow{}^4A_2(F)$ near 760 nm, such as in $MgWO_4$ [25] and $LiCoPO_4$ [26]. However, there is no absorption band near 760 nm in $Ba_{0.956}Mg_{0.912}Al_{10.088-x}Co_xO_{17}$. Three transitions at 553 nm, 587 nm, and 626 nm were observed in the visible light range (Fig. 6b). In this way, the assignments are consistent with the Tanabe-Sugano (TS) diagram for the d^7 electron configuration in a tetrahedral crystal field (Fig. 7). The absorption profiles are in agreement with the spectral features of $Co_xZn_{1-x}Al_2O_4$ [27] and $CoAl_2O_4/Al_2O_3$ composite [28], in which Co^{2+} states in a tetrahedral environment and presented three spin-allowed transitions, where $^4A_2(F)$ is a ground state. Therefore, three bands (553 nm, 587 nm, and 626 nm) located at visible light region can be attributed to the spin-allowed $^4A_2(F)\rightarrow{}^4T_1(P)$ transition, which is the origin of the ocean blue color. The other two spin-allowed transitions are $^4A_2(F)\rightarrow{}^4T_1(F)$ and $^4A_2(F)\rightarrow{}^4T_2(F)$ located at around 1324 nm and 1530 nm in the NIR region, respectively.

3.2. Analysis of blue zirconia ceramics

3.2.1. XRD analysis

The XRD patterns of the as-fired zirconia ceramics are shown in

Table 3
CIE value, digital photo, and the mass fraction of Ni/Co of as-fired zirconia ceramics.

Ceramic	The value of CIE			Digital photo	The mass fraction of Ni/Co
	L^*	a^*	b^*		
ZrO_2	89.96	-0.32	2.44		
5 wt% $Ba_{0.956}Mg_{0.912}Al_{9.988}Ni_{0.1}O_{17}$ + 95 wt% ZrO_2	83.76	-12.17	-8.53		0.04 wt%
10 wt% $Ba_{0.956}Mg_{0.912}Al_{9.988}Ni_{0.1}O_{17}$ + 90 wt% ZrO_2	83.47	-12.54	-12.05		0.08 wt%
5 wt% $Ba_{0.956}Mg_{0.912}Al_{9.888}Co_{0.2}O_{17}$ + 95 wt% ZrO_2	66.49	-5.87	-22.62		0.08 wt%
10 wt% $Ba_{0.956}Mg_{0.912}Al_{9.888}Co_{0.2}O_{17}$ + 90 wt% ZrO_2	66.73	-5.97	-25.79		0.17 wt%
5 wt% $CoAl_2O_4$ + 95 wt% ZrO_2	45.06	-1.48	-9.48		1.66 wt%
10 wt% $CoAl_2O_4$ + 90 wt% ZrO_2	46.01	-0.91	-6.32		3.33 wt%

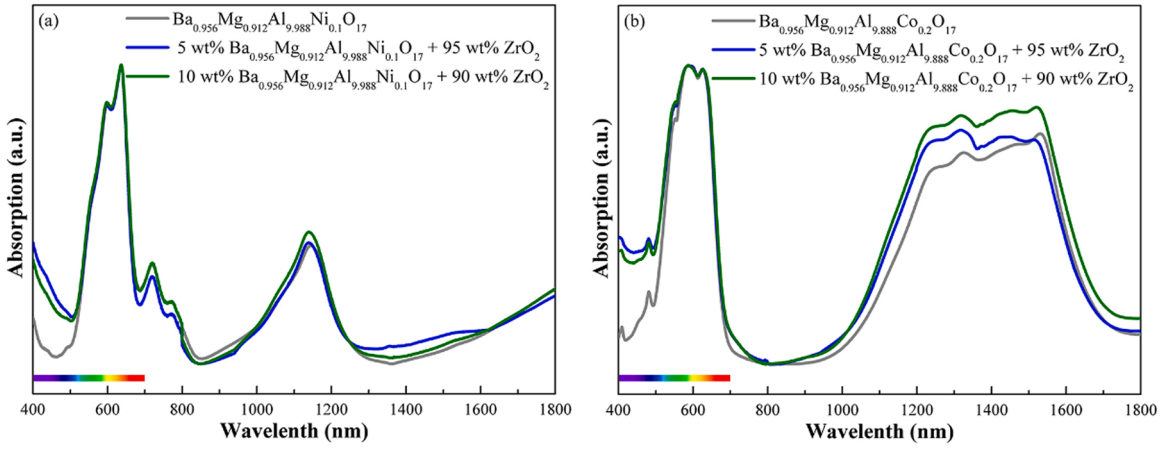

Fig. 12. The absorbance spectra of $Ba_{0.956}Mg_{0.912}Al_{9.988}Ni_{0.1}O_{17}$, $Ba_{0.956}Mg_{0.912}Al_{9.888}Co_{0.2}O_{17}$, and as-fired blue zirconia ceramics.

Fig. 8. After sintering, the as-synthesized zirconia ceramics completely transform to tetragonal zirconia (t-ZrO_2) with the space group of $P4_2/nmc$. The peaks of Ni/Co doped $Ba_{0.956}Mg_{0.912}Al_{10.088}O_{17}$ compounds are fairly weak due to the small amount of pigment compared to ZrO_2 in the ceramics. Though weak, the characteristic peaks of Ni/Co doped $Ba_{0.956}Mg_{0.912}Al_{10.088}O_{17}$ are observed at positions (107) ($2\theta = 33.2°$) and (114) ($2\theta = 35.6°$), as illustrated in Fig. 8b. Additionally, the peak intensity of $Ba_{0.956}Mg_{0.912}Al_{10.088}O_{17}$ peaks is stronger when changing the mass fraction of blue pigment from 5 wt% to 10 wt%. These indicate that either $Ba_{0.956}Mg_{0.912}Al_{9.988}Ni_{0.1}O_{17}$ or $Ba_{0.956}Mg_{0.912}Al_{9.888}Co_{0.2}O_{17}$ could stably exist in the ZrO_2 matrix at the sintering temperature of 1400 °C.

3.2.2. Microstructure analysis

The clear grains and their boundaries are observed under SEM (Fig. 9a, c). The grains show a particle distribution between 100 nm and 500 nm. For $Ba_{0.956}Mg_{0.912}Al_{9.988}Ni_{0.1}O_{17}$ zirconia ceramic, according to the EDS results summarized in Table 1, the dark grains (point 1) mainly consist of Al, O, as well as a small amount of Ba and Mg. The ratio of Ba:Mg:Al is close to the theoretical value of $Ba_{0.956}Mg_{0.912}Al_{9.988}Ni_{0.1}O_{17}$. Nevertheless, the trace of Ni/Co is hard to detect with EDS microanalyses, because the mass fraction of Ni/Co in as-prepared blue zirconia ceramics is less than 0.1 wt% (the minimum detection limit of the EDS instrument). Additionally, the shape of dark grains in the SEM image (Fig. 9a) overlays with the EDS elemental analysis of Al in $Ba_{0.956}Mg_{0.912}Al_{9.988}Ni_{0.1}O_{17}$ (Fig. 9b). Therefore, the dark grains are determined to be $Ba_{0.956}Mg_{0.912}Al_{9.988}Ni_{0.1}O_{17}$. All of these results show that two phases of $Ba_{0.956}Mg_{0.912}Al_{9.988}Ni_{0.1}O_{17}$ and ZrO_2 could coexist. Similar results are also observed in 5 wt% $Ba_{0.956}Mg_{0.912}Al_{9.888}Co_{0.2}O_{17}$ with 95 wt% ZrO_2 blue zirconia ceramic from the results of point 2 in Table 1, as well as Fig. 9c-d. So the as-prepared Ni/Co doped $Ba_{0.956}Mg_{0.912}Al_{10.088}O_{17}$ phase is stable after high-temperature sintering with ZrO_2.

3.2.3. XCT analysis

3D XCT reconstructions of as-fired zirconia ceramics show the pore distribution (Fig. 10) within an observation volume of $1.5 \times 1.5 \times 5$ mm^3. The left color bar indicates the volume of the pores.

Specifically, the pores in blue colors are small in size while the red color represents larger holes. It can be seen that the pores are independent spheres and are randomly distributed in the total scanned volume of all samples. The limited number and the small size of the pore show that the structure of as-synthesized zirconia ceramics is dense. No significant difference in pore distribution is observed when comparing the pore distribution of pure ZrO_2 ceramic and blue zirconia ceramics.

3.2.4. Mechanical properties

The Vickers hardness of the as-prepared zirconia ceramics was shown in Fig. 11 and summarized in Table 2. For each sample, measurements were taken on 14 different points on the polished ceramic surface. The hardness values of blue zirconia ceramics demonstrate a slight increase compared with those of the pure ZrO_2 ceramic, indicating that the hardness is slightly enhanced with the addition of the pigment phase. Furthermore, the differences of standard deviation were fairly small either on pure zirconia or blue zirconia, indicating a homogeneous microstructure. All the hardness value of as prepared ceramics exceeds 12 GPa of fully dense 3Y-TZP (3 mol% Yttria-stabilized Tetragonal Zirconia Polycrystal) [29], which meets the application requirements.

3.2.5. Optical properties

The CIE value, digital photos, and the mass fraction of Ni/Co of as-fired zirconia ceramics are presented in Table 3. The pure ZrO_2 ceramic presents a pure white color. When $Ba_{0.956}Mg_{0.912}Al_{9.988}Ni_{0.1}O_{17}$ pigment is introduced, the color of ceramic is tuned to sky blue. The ceramic appears ocean blue with the addition of $Ba_{0.956}Mg_{0.912}Al_{9.888}Co_{0.2}O_{17}$ pigment. In both $Ba_{0.956}Mg_{0.912}Al_{9.888}Co_{0.2}O_{17}$ and $Ba_{0.956}Mg_{0.912}Al_{9.988}Ni_{0.1}O_{17}$ zirconia materials, the results show that with the pigment fraction increasing from 5 wt% to 10 wt%, the lightness value L^* and the redness value a^* is stable while the yellowness value b^* decreases. For a comparison, cobalt blue powders and their zirconia ceramic are synthesized following the same solid state reaction route. As shown in Table 3, the as-prepared cobalt blue zirconia ceramics show a less blue hue and heavier darkness which corresponds to a higher b^* value (−9.48) and a lower L^* value (45.06). So for the synthesis of blue zirconia based on cobalt blue, complicated procedures such as injection molding and solution infiltration method [30] as well as heterogeneous nucleation method [31] must be employed to maintain an intense blue color. While in Co/Ni doped $Ba_{0.956}Mg_{0.912}Al_{10.088}O_{17}$ based blue zirconia prepared by simple solid state reaction, the blue zirconia ceramics show almost the same intense blue colors as its pigment powder, indicating a simplification in the blue zirconia ceramic synthesis. Moreover, the mass fraction of Co in 5 wt% $CoAl_2O_4$ zirconia ceramic is 1.66 wt%, which is almost 20 times higher than that in 5 wt% $Ba_{0.956}Mg_{0.912}Al_{9.888}Co_{0.2}O_{17}$ zirconia ceramic (0.08 wt%). Therefore, $Ba_{0.956}Mg_{0.912}Al_{9.888}Co_{0.2}O_{17}$ is a promising pigment in the blue zirconia ceramic synthesis with advantages of low Co content and an easily-achieved synthesis procedure.

The absorbance spectra of $Ba_{0.956}Mg_{0.912}Al_{9.988}Ni_{0.1}O_{17}$ and $Ba_{0.956}Mg_{0.912}Al_{9.888}Co_{0.2}O_{17}$ blue pigments powder, as well as as-fired blue zirconia ceramics, are given in Fig. 12. The peak positions of the blue pigments and blue zirconia ceramics are similar, which indicates that the color origin of the blue zirconia ceramic is the same as its pigment. Based on the optical characterizations of the blue zirconia blocks, ZrO_2 could be tuned to a blue color with a small amount of pigment.

4. Conclusions

In summary, the Ni/Co doped $Ba_{0.956}Mg_{0.912}Al_{10.088}O_{17}$ blue pigments were successfully synthesized by a solid state reaction. The UV-Vis-NIR spectra revealed the color mechanism of the as-synthesized pigment is *d-d* transitions from the doped transition metal ions. For $Ba_{0.956}Mg_{0.912}Al_{10.088-x}Ni_xO_{17}$ ($0 \le x \le 0.3$), the origin of sky blue is attributed to the spin-allowed transition of $^3T_1(F) \rightarrow {}^3T_1(P)$ (600 nm and 637 nm) from Ni^{2+} in tetrahedral coordination. The ocean blue color of $Ba_{0.956}Mg_{0.912}Al_{10.088-x}Co_xO_{17}$ ($0 \le x \le 0.3$) is associated with the spin-allowed $^4A_2(F) \rightarrow {}^4T_1(P)$ transition (553 nm, 587 nm, and 626 nm) from Co^{2+} in a tetrahedral site. Then, the blue zirconia ceramics containing 5 wt% and 10 wt% as-synthesized blue pigments were prepared at 1400 °C via a solid state method. Confirmed by both XRD and SEM analysis, the pigment phase is maintained after high-temperature sintering with ZrO_2. Based on the XCT and Vickers hardness results, the blue zirconia ceramics are dense, and the mechanical properties of the fabricated blue ceramics were maintained compared to pure ZrO_2 ceramic. With a lower amount of Co as well as a simple ceramic synthesis procedure, the as-prepared novel Ni/Co doped $Ba_{0.956}Mg_{0.912}Al_{10.088}O_{17}$ blue pigments are proved to be promising colorants for blue zirconia ceramics.

Declaration of Competing Interest

There are no conflicts of interest to declare.

Acknowledgments

This work was supported by the National Natural Science Foundation of China under Grant No. 51872023, and Fundamental Research Funds for the Central Universities and the Youth Teacher International Exchange & Growth Program under the grant No. FRF-MP-20–28 and No. QNXM20210020. The work done at Oregon State University is supported by US National Science Foundation Grant No. DMR-2025615.

References

[1] F. Zarone, S. Russo, R. Sorrentino, From porcelain-fused-to-metal to zirconia: Clinical and experimental considerations, Dent. Mater. 27 (1) (2011) 83–96.
[2] H. Lv, J. Bao, S. Qi, Q. Jin, W. Guo, Optical and mechanical properties of purple zirconia ceramics, J. Asian Ceram. Soc. 7 (3) (2019) 306–311.
[3] F. Ren, S. Ishida, N. Takeuchi, Color and vanadium valency in V-doped ZrO_2, J. Am. Ceram. Soc. 76 (7) (1993) 1825–1831.
[4] M. Ocaña, A.R. González-Elipe, M. Andrés-Vergés, P. Tartaj, C.J. Serna, V.M. Orera, Preparation by hydrolysis of aerosols and colour properties of Cr-doped and Co-doped zircon powders, J. Eur. Ceram. Soc. 18 (7) (1998) 821–830.
[5] H. Lv, J. Bao, F. Ruan, F. Zhou, Q. Wang, W. Zhang, W. Guo, Y. Zhang, X. Song, S. An, Preparation and properties of black Ti-doped zirconia ceramics, J. Mater. Res. Technol. 9 (3) (2020) 6201–6208.
[6] H. Lv, J. Bao, L. Chao, X. Song, S. An, F. Zhou, Q. Wang, F. Ruan, W. Zhang, W. Guo, Y. Zhang, Development mechanism of Ce-doped red zirconia ceramics prepared by a high-temperature reduction method, J. Alloy. Compd. 797 (2019) 931–939.
[7] T. Zhang, J. Huang, J. Yan, X. Yin, Y. Wang, Pigments based on Er_2O_3-Al_2O_3: Preparation and colouring performance in zirconia ceramics, Ceram. Int. 46 (11) (2020) 17523–17531.
[8] E. Sani, D. Sciti, C. Capiani, L. Silvestroni, Colored zirconia with high absorbance and solar selectivity, Scr. Mater. 186 (2020) 147–151.
[9] J. Zhang, Z. Zhang, Z. Tang, Z. Zheng, Y. Lin, Synthesis and characterization of $BaMgAl_{10}O_{17}$: Eu phosphors derived by sol-gel processing, Powder Technol. 126 (2) (2002) 161–165.
[10] N.T. Huyen, N. Tu, D.T. Tung, D.Q. Trung, D.D. Anh, D.T. Thien, T.T.T. Nga, H. Pham, Photoluminescent properties of red-emitting phosphor $BaMgAl_{10}O_{17}$: Cr^{3+} for plant growth LEDs, Opt. Mater. 108 (2020), 110207.
[11] M. Kumar, P. Rajput, P.K. Singh, A.C. Yadav, S.L. Pradhan, V. Baranwal, U. B. Singh, S.N. Jha, F. Singh, Luminescence properties of $BaMgAl_{10}O_{17}$: Mn^{2+} nanophosphors, J. Alloy. Compd. 799 (2019) 556–562.
[12] S. Kunimi, S. Fujihara, Elaboration of blue-emitting blue pigments based on Eu^{2+}/Co^{2+} codoped $BaMgAl_{10}O_{17}$ through the heterogeneous distribution of dopants, Dyes Pigments 91 (1) (2011) 49–54.
[13] M. Bellotto, G. Artioli, C. Cristiani, P. Forzatti, G. Groppi, On the crystal structure and cation valence of Mn in Mn-substituted Ba-β-Al_2O_3, J. Catal. 179 (2) (1998) 597–605.
[14] N. Iyi, Z. Inoue, S. Kimura, The crystal structure and cation distribution of highly nonstoichiometric magnesium-doped potassium β-alumina, J. Solid State Chem. 61 (2) (1986) 236–244.
[15] H.W. Nesbitt, D. Legrand, G.M. Bancroft, Interpretation of Ni2p XPS spectra of Ni conductors and Ni insulators, Phys. Chem. Miner. 27 (2000) 357–366.
[16] T.H. Gardner, J.J. Spivey, E.L. Kugler, A. Campos, J.C. Hissam, A.D. Roy, Structural characterization of Ni-substituted hexaaluminate catalysts using EXAFS, XANES, XPS, XRD, and TPR, J. Phys. Chem. C. 17 (114) (2010) 7888–7894.

[17] Y. Wang, Q. Cheng, P. Jiang, L. Liu, K. Cui, Y. Li, Synthesis and properties of novel blue zirconia ceramic based on Co/Ni-doped $BaAl_{12}O_{19}$ blue chromophore, J. Eur. Ceram. Soc. 42 (2) (2022) 543–551.

[18] J.-I. Jung, D.D. Edwards, X-ray photoelectron (XPS) and Diffuse Reflectance Infra Fourier Transformation (DRIFT) study of $Ba_{0.5}Sr_{0.5}Co_xFe_{1-x}O_{3-\delta}$ (BSCF: x=0-0.8) ceramics, J. Solid State Chem. 184 (8) (2011) 2238–2243.

[19] N.S. Mcintyre, M.G. Cook, X-ray photoelectron studies on some oxides and hydroxides of cobalt, nickel, and copper, Anal. Chem. 47 (13) (1975) 2208–2213.

[20] J.G. Dillard, C.V. Schenck, M.H. Koppelman, Surface chemistry of cobalt in calcined cobalt-kaolinite materials, Clays Clay Miner. 31 (1) (1983) 69–72.

[21] M. Dondi, T.S. Lyubenova, J.B. Carda, M. Ocaña, M-doped Al_2TiO_5 (M=Cr, Mn, Co) solid solutions and their use as ceramic pigments, J. Am. Ceram. Soc. 92 (9) (2009) 1972–1980.

[22] S. Wang, H. Gao, L. Fang, Y. Wei, Y. Li, L. Lei, Synthesis and characterization of $BaAl_2O_4$ catalyst and its photocatalytic activity towards degradation of methylene blue dye, Z. für Phys. Chem. 233 (8) (2019) 1161–1181.

[23] G. Costa, M.J. Ribeiro, W. Hajjaji, M.P. Seabra, J.A. Labrincha, M. Dondi, G. Cruciani, Ni-doped hibonite ($CaAl_{12}O_{19}$): A new turquoise blue ceramic pigment, J. Eur. Ceram. Soc. 29 (13) (2009) 2671–2678.

[24] M. Ardit, S. Borcănescu, G. Cruciani, M. Dondi, I. Lazău, C. Păcurariu, C. Zanelli, J. McKittrick, Ni-Ti codoped hibonite ceramic pigments by combustion synthesis: Crystal structure and optical properties, J. Am. Ceram. Soc. 99 (5) (2016) 1749–1760.

[25] D. Saraswathy, P.P. Rao, A.K.V. Raj, T.R.A. Thara, Intense blue colors in wolframite-type Co^{2+}: $MgWO_4$ oxides through distortion in Co^{2+} octahedra, ChemistrySelect 3 (2) (2018) 410–417.

[26] B. Serment, L. Corucho, A. Demourgues, G. Hadziioannou, C. Brochon, E. Cloutet, M. Gaudon, Tailoring the chemical composition of $LiMPO_4$ (M = Mg, Co, Ni) orthophosphates to design new inorganic pigments from magenta to yellow hue, Inorg. Chem. 58 (11) (2019) 7499–7510.

[27] L. Desouza, J. Zamian, G. Darochafilho, L. Soledade, I. Dossantos, A. Souza, T. Scheller, R. Angelica, C. Dacosta, Blue pigments based on $Co_xZn_{1-x}Al_2O_4$ spinels synthesized by the polymeric precursor method, Dyes Pigments 81 (3) (2009) 187–192.

[28] X. He, W. Zhu, X. Wang, F. Wang, H. Liu, Z. Lei, Synthesis and color properties of the $CoAl_2O_4/Al_2O_3$ hybrid blue pigments with low cobalt contents, J. Mater. Sci. 55 (28) (2020) 13569–13577.

[29] J. Chevalier, S. Deville, E. Munch, R. Jullian, F. Lair, Critical effect of cubic phase on aging in 3 mol% yttria-stabilized zirconia ceramics for hip replacement prosthesis, Biomaterials 25 (24) (2004) 5539–5545.

[30] G. Liu, Z. Xie, W. Wang, Y. Wu, Fabrication of ZrO_2-$CoAl_2O_4$ composite by injection molding and solution infiltration, Int. J. Appl. Ceram. Technol. 8 (6) (2011) 1344–1352.

[31] W. Wang, Z. Xie, G. Liu, W. Yang, Fabrication of blue-colored zirconia ceramics via heterogeneous nucleation method, Cryst. Growth Des. 9 (10) (2009) 4373–4377.